Equivalent Voice-coil Models for Real-time Computation in Electromagnetic Actuation and Sensor Applications

Kok-Meng Lee*, *Fellow*, *IEEE* and Hungsun Son

Abstract— **This paper presents a method to derive equivalent models to characterize the magnetic field of a multi-layer (ML) voice coil. Two equivalent models are discussed. The first reduces the number of wire layers to a minimum. To offer some intuitive insights, a detailed derivation of an equivalent single layer (ESL) model is given in this paper. The second models the ML coil as an equivalent PM, the magnetic field of which has a closed-form solution. The equivalent models are validated by investigating the effects of coil geometry on the modeling errors, and by comparing the computed forces against published data. As illustrated with a number of examples in this paper, the field and force calculations which do not increase with the number of current loop-turns offer a number of advantages in real-time applications.**

Index Terms— **Electromagnetic field modeling, Lorentz force, actuator design, spherical motor**

I. Introduction

Iron-less voice coils are commonly used in mechatronic devices (such as hard-disk drives and multi-DOF actuators) due to their linearity as they are free from iron saturation, and the wide availability of high-coercive rare-earth permanent magnets at low cost. The ability to calculate the magnetic fields and forces in real-time can offer a number of advantages. These include accounting for the effects of the self and mutual inductances of the voice coils and the back electromotive forces (emf) on the voltage controlled devices, as well as offering effective motion estimation for model-based control of electromagnetic actuators.

Magnetic forces exerted on current-carry conductors in a magnetic field are often calculated by the use of Lorentz force equation, which does not involve the magnetic flux generated by the current loop as the current density vector is directly used in the calculation. However, the three-dimensional (3D) integral of the Lorentz force equation must account for each of the current-carrying conductors. For devices such as a spherical motor [1]-[5] where a large number of coils (with multi layers of wires in each) are used, the field and force calculations are often very time consuming for real time applications. A common approach to accurately compute the magnetic fields has been the use of numerical methods such as FEM. Numerical methods such as FEM offer a good prediction of the magnetic field for accurate computation of the magnetic torque. However, demanding computational time limits these numerical methods to off-line computation.

Manuscript received on June 30, 2007. This work was jointly supported by the Georgia Agricultural Technology Research Program (ATRP) and the U. S. Poultry and Eggs Association. The authors are with the Woodruff School of Mechanical Engineering, Georgia Institute of Technology

* Corresponding author: kokmeng.lee@me.gatech.edu; tel: +1(404)894-7402; fax: +1(404)894-9342.

In [6], we introduce an alternative method, referred here as distributed multi-pole (DMP) modeling, to compute the magnetic fields of permanent magnets using a distributed set of dipoles enabling the magnetic flux density to be computed in closed form. The concept of a magnetic dipole is also commonly used to characterize the magnetic field of a single circular loop carrying current. However, unlike the magnetic dipole [7] derived on the basis of a vector potential for a single current loop, the equivalent models introduced here take into account the physical dimension of a multi-layer coil in modeling the magnetic fields. Yet, as in the case of a magnetic dipole the equivalent PM model of the coil offers the field solutions in closed form. Once the magnetic fields of both the permanent magnets and voice coils are obtained in closed form, they can be computed in real-time for motion estimation.

In this paper, two equivalent models to reduce computation time for calculating the magnetic fields and forces involving multilayer (ML) voice coils are introduced; an equivalent single layer (ESL) model, and an equivalent permanent magnet (PM) model. The first method (or the ESL model) reduces the original ML voice coil to an equivalent model, which retains the shape of the original coil but with only a minimum number of wire layers. The second method models the original ML voice coil, as an equivalent PM which can then be characterized by a distributed set of magnetic dipoles or simply the DMP [6] model. The DMP model inherits many advantages of the dipole model originally conceptualized in the context of physics [8]-[12], but provides an effective means to account for the shape and magnetization of the physical magnet. As will be shown, the field and force calculations do not increase with the number of turns once the equivalent model is found.

The remainder of this paper offers the following:

1) We formulate and derive two equivalent models for efficient computing the magnetic flux density of a voice coil. The key to this method is to find an effective radius and current density (or a magnetization vector for the case of an equivalent PM) such that the equivalent models closely approximates the magnetic flux density.
2) We validate the equivalent model by investigating the effects of coil geometry on the modeling errors, and by comparing the computed forces against published data.
3) We illustrate two applications of the equivalent PM model; a pole-shape design and field-based orientation sensing. Unlike numerical solutions such as finite element methods, the magnetic field solutions obtained using the equivalent PM model are in closed form and thus well suit for real-time computational applications.

1-4244-1264-1/07/$25.00 ©2007 IEEE

II. Equivalent Models of a Multi-layer Voice Coil

The design of electromagnetic actuators and sensors involves calculation of magnetic fields and forces due to a current-carrying voice coil. For a thin wire with cross-section area S, the magnetic field density caused by the current I flowing along the wire can be determined by the Biot-Savart law:

$$\mathbf{B}_s = \oint d\mathbf{B}_s \quad \text{where } d\mathbf{B}_s = \frac{\mu_o I}{4\pi} \frac{d\mathbf{s}\times\mathbf{e}_R}{\left|\mathbf{R}-\mathbf{R}'\right|^2} \tag{1}$$

where $d\mathbf{s}$ is an elemental length vector of the wire; $\mathbf{e}_R$ is the unit vector from the source point $\mathbf{R}'$ to the field point $\mathbf{R}$; $I = \oint_S JdS$; J is the current density; and μ_0 is free space permeability. The Lorentz force exerted on the current-carry conductor due to the magnetic flux density $\mathbf{B}_r$ can be calculated using (2):

$$\mathbf{F} = -\oint \mathbf{B}_r \times Id\mathbf{n} \quad \text{where } I = \oiint \mathbf{J}\bullet d\mathbf{S} \tag{2}$$

where $d\mathbf{n}$ is the normalized current direction vector.

In (1) and (2), the integral must account for each of the current-carrying conductors. An effective method to reduce computation time is to replace the multilayer (ML) coil with an equivalent single-layer (ESL) model. In general, the ESL model retains the shape of the original ML coil but with only one layer of wires. For example, for a cylindrical coil the process involves finding an effective radius a_e and current density J_e. The unknown parameters are chosen such that the errors of the magnetic flux along the centroidal axis are minimized, and that the same magnetic flux density is generated at the end surface of the core. As will be shown, the field and force calculations of the ESL model do not increase with the number of turns.

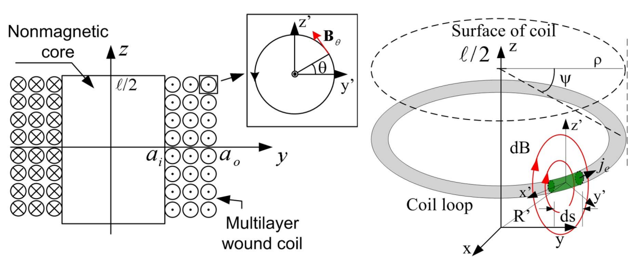

(a) Cross sectional view (b) Magnetic flux on the wire

Fig. 1 Multilayer voice coil

Without loss of generality, we illustrate the modeling method with concentric coils as shown in Fig. 1(a), where some analytical solutions are available for model validation. However, the method can be extended to coils of other customized shape.

A. Equivalent Single-layer (ESL) Model

Consider a typical multilayer (axi-symmetrical) coil with a current density J, the sectional view of which is shown in Fig. 1(a). The current flowing in the wire towards the $+x$-axis generates a circular magnetic flux. As a result, the cumulative magnetic fluxes reverse its direction from $y=0$ to the location $a_i<y<a_o$. The radial location (where the flux reverses its direction) is called switching radius ρ and is a function of z.

To find the switching radius, we consider the 2D magnetic flux density as shown in Fig. 1(a). For a single wire,

$$\mathbf{B}(y',z') = \frac{\mu_0}{2\pi r}(\mathbf{I}\times\mathbf{e}_r) \ \text{ where } \mathbf{I} = I\mathbf{e}_x \text{ and } I = \int_S JdS . \tag{3}$$

The total magnetic flux densities at any point (distance vector $\mathbf{R}$) can be calculated by integrating over the current-carrying conductor. For the original ML coil (with inner and outer radii, a_i and a_o, respectively)

$$\mathbf{B}_{ML}(y,z) = \frac{\mu_0 J}{2\pi}\int_{-\ell/2}^{\ell/2}\left(\int_{a_i}^{a}\frac{1}{\left|\mathbf{R}-\mathbf{R}'\right|} + \int_{-a_i}^{-a_o}\frac{1}{\left|\mathbf{R}-\mathbf{R}'\right|}\right)dy'dz'\mathbf{e}_\theta \tag{4a}$$

where $\mathbf{e}_\theta = -\sin\theta\mathbf{e}_y + \cos\theta\mathbf{e}_z$ and $\left|\mathbf{R}-\mathbf{R}'\right| = \sqrt{(y-y')^2+(z-z')^2}$. Similarly, for a single layer coil,

$$\mathbf{B}_{SL}(y,z) = \frac{\mu_0 J_e d_w}{2\pi}\int_{-\ell/2}^{\ell/2}\frac{1}{\left|\mathbf{R}-\mathbf{R}'_+\right|} + \frac{1}{\left|\mathbf{R}-\mathbf{R}'_-\right|}dz'\mathbf{e}_\theta \tag{4b}$$

where $\left|\mathbf{R}-\mathbf{R}'_\pm\right| = \sqrt{(y\mp a_e)^2+(z-z')^2}$. As the magnetic flux is dominant along the centroidal axis, the unknown parameters (J_e and a_e) are determined to satisfy two conditions:

<u>Condition I</u>: Minimize the difference between the two models defined by (5):

$$E_y = \int_0^\infty \left|B_{Mz}(y,z) - B_{Sz}(y,z)\right|_{z=\ell/2} dy \tag{5}$$

where $B_{Mz}(y,z) = \mathbf{B}_{ML}(y,z)\bullet\mathbf{e}_z$ and $B_{Sz}(y,z) = \mathbf{B}_{SL}(y,z)\bullet\mathbf{e}_z$

Note that $\cos\theta = (y-y')/\left|\mathbf{R}-\mathbf{R}'\right|$, we have

$$\frac{B_{Mz}(y,\ell/2)}{\mu_0 J\ell/(2\pi)} = \tag{5a}$$

$$\frac{1}{2}\ln\left[\left(\frac{1+\chi_{i-}^2}{1+\chi_{o-}^2}\right)\left(\frac{1+\chi_{i+}^2}{1+\chi_{o+}^2}\right)\right] + \chi_{i-}\vartheta_{i-} - \chi_{o-}\vartheta_{o-} + \chi_{i+}\vartheta_{i+} - \chi_{o+}\vartheta_{o+}$$

$$\frac{B_{Sz}(y,\ell/2)}{\mu_0 J\ell/(2\pi)} = -\frac{J_e d_w}{J\ell}\left(\cot^{-1}\chi_{e-} + \cot^{-1}\chi_{e+}\right) \tag{5b}$$

where $\chi_\pm = (a\pm y)/\ell$; $\vartheta = \cot^{-1}\chi$; and the subscripts i, o, and e denote inner, outer and effective radius respectively.

<u>Condition II</u>: The effective current density J_e is determined such that $B_{ML}(0,\pm\ell/2) = B_{SL}(0,\pm\ell/2)$

$$J_e d_w = \frac{J\ell}{\cot^{-1}(a_e/\ell)}\left[\chi_o\cot^{-1}\chi_o - \chi_i\cot^{-1}\chi_i - \frac{1}{2}\ln\left(\frac{1+\chi_i^2}{1+\chi_o^2}\right)\right] \tag{6}$$

where $\chi_i = a_i/\ell$; $\chi_o = a_o/\ell$ and $\chi_e = a_e/\ell$.

The unknown parameters (a_e and J_e) can be solved simultaneously from (5) and (6). For an axi-symmetrical coil, a 2D model as shown in Fig. 1(a) is sufficient for deriving the unknown parameters of the ESL model. However, the 3D magnetic flux density is needed for field calculation, which can be obtained by applying the Biot-Savart law in (7). For the original ML coil,

$$\mathbf{B}_{ML} = -\frac{\mu_o J}{4\pi}\left[\int_{-\ell/2}^{\ell/2}\int_{a_i}^{a_o}\int_0^{2\pi}\frac{\left[\mathbf{R}-\mathbf{R}'\right]\times rd\boldsymbol{\theta}}{\left|\mathbf{R}-\mathbf{R}'\right|^3}drdz'\right]\mathbf{e}_\psi \tag{7}$$

where $\left|R-R'\right| = (x-r\cos\theta)^2 + (y-r\sin\theta)^2 + (z-z')^2$;

1-4244-1264-1/07/$25.00 ©2007 IEEE

$$\mathbf{e}_\psi = -\sin\psi\mathbf{e}_\mathbf{y} + \cos\psi\mathbf{e}_\mathbf{k}\text{; and}$$

$$\psi = \cos^{-1}\left(\sqrt{(x-r\cos\theta)^2+(y-r\sin\theta)^2}\,/\left|\mathbf{R}-\mathbf{R}'\right|\right).$$

In (7), the negative sign is due to the cross product in the coordinate system of Fig. 1(b). Similarly, once a_e and J_e are found the 3D magnetic flux density can be derived from the equivalent single layer (ESL) model:

$$\mathbf{B}_{SL} = \frac{-\mu_o J_e d_w}{2\pi}\left[\int_{-\ell/2}^{\ell/2}\int_0^{2\pi}\frac{[\mathbf{R}-\mathbf{R}']\times a_e d\boldsymbol{\theta}}{\left|\mathbf{R}-\mathbf{R}'\right|^3}dz'\right]\mathbf{e}_\psi \tag{8}$$

B. Equivalent PM Model

The ESL model significantly reduces the computation time of the Lorentz force; however, the magnetic flux density must be integrated numerically. For real-time applications, it is desired to have the magnetic field solutions in closed form; this can be achieved by modeling the coil as an equivalent permanent magnet (PM) with an effective radius a_e, length ℓ, and an effective magnetization vector $\mathbf{M}_e = M_o\mathbf{e}_\mathbf{z}$), the magnetic field solutions of which can then be presented in closed form using distributed multiple dipoles (DMP) [6]. The effective magnetization vector $\mathbf{M}_e$ is determined to satisfy the following condition:

$$B_{Pz} = \mathbf{B}(0,0,\ell/2)\bullet\mathbf{e}_z \tag{9}$$

where $\mathbf{B}(0,0,\ell/2)$ is the magnetic field of the original coil. For a field that is continuous ($\nabla\bullet\mathbf{B}=0$) and irrotational ($\nabla\times\mathbf{B}=0$), a scalar magnetic potential Φ can be defined such that the magnetic intensity $\mathbf{H} = -\nabla\Phi$. The general expression [13] of Φ_A from a magnetic surface charge at $\mathbf{R}'(x', y', z')$ to the field point $\mathbf{R}(x, y\, z)$ is given in (10):

$$\Phi_A = \frac{1}{4\pi}\int_V\frac{-\nabla\bullet\mathbf{M}}{\left|\mathbf{R}-\mathbf{R}'\right|}dV + \frac{1}{4\pi}\int_S\frac{\mathbf{M}\bullet\mathbf{n}}{\left|\mathbf{R}-\mathbf{R}'\right|}dS \tag{10}$$

The corresponding magnetic flux density can be derived from the constitutive relation $\mathbf{B} = \mu_0\mathbf{H}$. For a cylindrical PM,

$$B_{Pz} = 0.5\mu_o M_o\left[1+\left(a_e/\ell\right)^2\right]^{-1/2} \tag{11}$$

The magnitude of the effective magnetization vector can then be obtained by equating (9) and (11):

$$\mu_o M_o = 2\sqrt{1+\left(a_e/\ell\right)^2}\,\mathbf{B}(0,0,\ell/2)\bullet\mathbf{e}_z \tag{12}$$

where $\mathbf{B}(0,0,\ell/2)$ can be computed from (8).

A closed-form solution approximating the magnetic field of the coil is given by the DMP model that has k circular loops of n dipoles with strength m_j (j = 0, 1, … , k) parallel to $\mathbf{M}_e$:

$$\mathbf{B}_{PM} = \frac{\mu_o}{4\pi}\sum_{j=0}^{k} m_j\sum_{i=1}^{n_k}\left(\frac{\mathbf{a}_{Rji+}}{R_{ji+}^2}-\frac{\mathbf{a}_{Rji-}}{R_{ji-}^2}\right)\text{ and } n_k = \begin{cases}1 & \text{if } j=0\\ n & \text{if } j\neq 0\end{cases} \tag{13}$$

where $\frac{\mathbf{a}_{Rji\pm}}{R_{ji\pm}^2} = -\frac{\left(x-\bar{a}_j\cos i\theta\right)\mathbf{a}_x+\left(y-\bar{a}_j\sin i\theta\right)\mathbf{a}_y+\left(z\mp\bar{\ell}/2\right)\mathbf{a}_z}{\left[\left(x-\bar{a}_j\cos i\theta\right)^2+\left(y-\bar{a}_j\sin i\theta\right)^2+\left(z\mp\bar{\ell}/2\right)^2\right]^{3/2}}$;

$\bar{\ell}$ is the distance between the source/ sink of the dipole; and $\bar{a}_j$ is the radius of the j^{th} loop. A general method for finding an optimized set of distributed dipole parameters ($\bar{a}_j$, $\bar{\ell}$, k, n, δ, and m_j) to characterize a PM can be found in [6].

III. Simulations and Model Validation

We present two sets of simulation results. The 1st set illustrates the ESL model, and examines its effects of coil geometries on the magnetic flux density and the Lorentz force. The 2nd simulation validates the equivalent models and compares the computed forces against published data.

A. ESL model and Effects of Coil Geometry

Table 1 compares three different coil geometries and their effects on the magnetic flux density for the same wire volume of 5.41 cm^3 and length $\ell = 25.4$mm .

Table 1: Effects of the ML coil geometry on ESL model

Geometry			Current density	% Error at $z=\ell/2+\varepsilon$	
a_i/a_o	a_o/ℓ	a_e/a_o	$J_e d_w$ (A/mm)	$\varepsilon=1\mu m$	$\varepsilon=1mm$
0.1	0.3256	0.582	137.1	32.0%	19.0%
0.5	0.3740	0.766	136.7	13.4%	6.6%
0.9	0.7437	0.951	136.2	1.3%	0.6%

Volume=5.41cm^3 (0.33 in^3); $\ell = 25.4$mm (1in); 29AWG wire with 4A current.

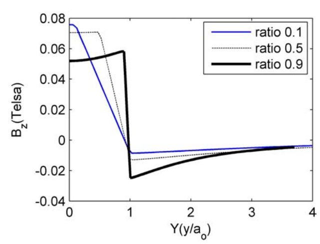

3(a) Original ML (ε=1μm)

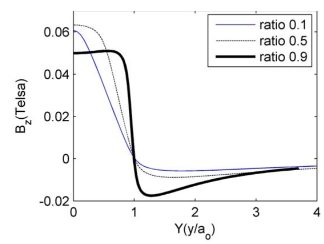

4(a) Original ML (ε=1mm)

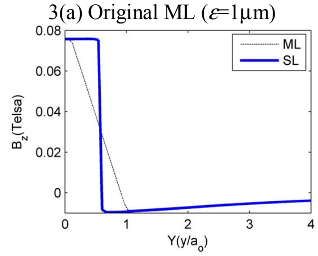

3(b) $a_i/a_o = 0.1$(ε=1μm)

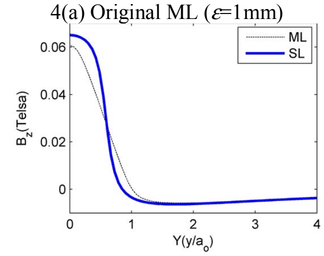

4(b) $a_i/a_o = 0.1$ (ε=1mm)

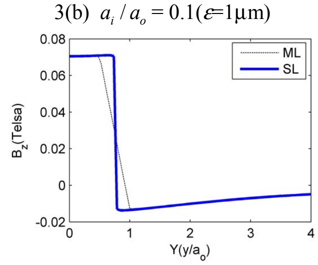

3(c) $a_i/a_o = 0.5$(ε=1μm)

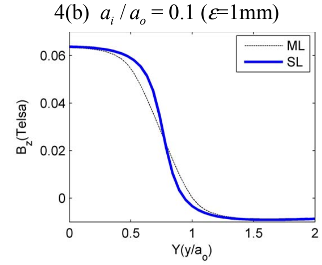

4(c) $a_i/a_o = 0.5$ (ε=1mm)

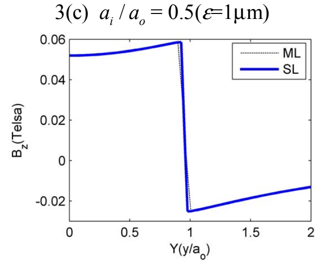

3(d) $a_i/a_o = 0.9$ (ε=1μm)

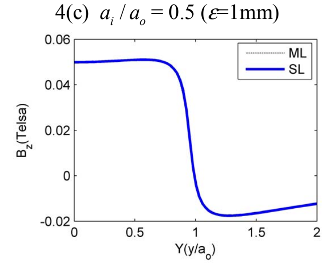

4(d) $a_i/a_o = 0.9$ (ε=1mm)

Fig. 3 $B_{Sz}(y,\ell/2+1\mu m)$

Fig. 4 $B_{Sz}(y,\ell/2+1mm)$

1-4244-1264-1/07/$25.00 ©2007 IEEE

With the current of 4 Amperes, the effective radius a_e and current density J_e in Table1 were found numerically using the optimization toolbox in MATLAB. Since the magnetic flux density of the ESL model is singular at the surface ($z = \ell/2$), we compare $B_{Sz}(y, \ell/2+\varepsilon)$ at ε=1μm and 1mm in Figs. 3 and 4 respectively for three different ratios a_i/a_o=0.1, 0.5 and 0.9. The errors of the ESL models are summarized in Table 1 where the % Error is defined as

$$\%\text{Error} = \left[\int_0^\infty \left| B_{Mz}(y,z) - B_{Sz}(y,z)\right|_{z=\ell/2} dy\right] \Big/ \left[\int_0^\infty \left| B_{Mz}(y,z)\right|_{z=\ell/2} dy\right]$$

Comparison of results in Fig. 3, Fig. 4 and Table 1 shows that the ESL model well approximates magnetic fields of coils with $a_i/a_o \geq 0.5$. As expected, discrepancies between the ML and ESL models occurs primary at the surface ($z = \ell/2$), particularly for coils with a very small a_i/a_o ratio. This implies that one or more additional wire layers may be needed to improve the approximation. For the same volume of wires and coil length, thin coils ($a_i/a_o \approx 1$) tend to have a more uniform but lower magnetic flux density along the centroidal axis than that of the thick coil ($a_i/a_i << 1$).

Figure 5(a) shows the setup used to compare the torque computed with the 3D field of the ESL model (8) against that based on the 3D field of the original ML coil (7), where the cylindrical PM is rotated in the *xz* plane towards the ML coil. The parameters of the PM and coil are given in Fig. 5(a). Computation with the ESL model requires only 5% of the computation time with the original ML coil in MATLAB. As shown in Fig. 5(b), the two computed torque are in excellent agreement.

Permanent magnet (PM):
$2a = \ell = 12.7$mm ; $\mu_0 M_0 = 1.27$ **T**
coil: 29AWG wire
a_o=9.5, a_i=4.76, $\ell = 25.4$mm
\# of turns = 1050; Current= 4A
Gap between PM and coil = 0.5mm

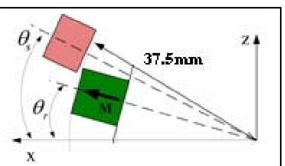

(a) Parameters used in simulation

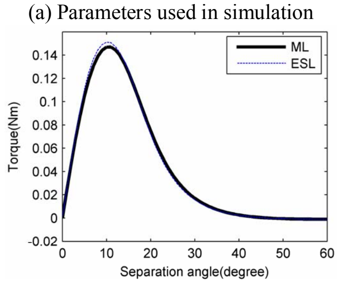

(b) Torque vs separation angle ($\theta_s - \theta_r$) with 3D fields

Fig. 5 Effect of equivalent models

B. ESL Model Validation with Force Computation

To validate the equivalent models, we model the setup in Fig. 6 (for two size combinations), where the parameters are summarized in Table 2. The computed forces are compared against published numerical [14] and experimental [15] data in Fig. 7, which graphs the magnetic flux density along the z-axis calculated using the ESL model and the original ML coil; the comparisons are remarkably close.

The magnetic forces (between a PM and a coil in Fig. 6) were computed using the Lorentz force (2) to calculate the magnetic force exerted on the original ML coil (7) and the equivalent SL model (8). The Lorentz force calculation involves only modeling the **B**-fields of the PM. However, once **B** field of the coil is known, the force on a body can also be computed from the surface integration in term of Maxwell stress tensor **T**:

$$\mathbf{F} = \oint_\Gamma \mathbf{T} d\Gamma \quad \text{where } \mathbf{T} = \frac{1}{\mu_0}\left(\mathbf{B}(\mathbf{B}\bullet\mathbf{n}) - \frac{1}{2}B^2\mathbf{n}\right); \tag{14}$$

where Γ is an arbitrary boundary enclosing the body of interest; and **n** is the normal of the material interface.

The modeled axial and tangential forces are compared in Figs. 7(a) and 7(b) respectively against published experimental data and numerical results computed using mesh-less method (MLM) [14]. As shown in Fig. 7, both (the original ML coil and equivalent SL model) agree very closely with each other and with the MLM. Maximum differences from the experimental data, $100\times|F_m - F_{\exp}|/|F_{\exp}|$, are within 10% as shown in Table 3.

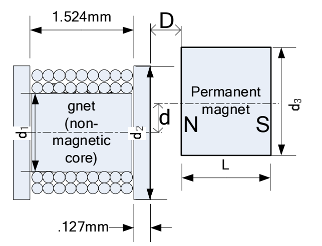

Size	Large	Small
d_1 (mm)	3.048	1.524
d_2 (mm)	3.962	3.175
d_3 (mm)	2.998	1.6
L (mm)	1.6	0.813
Coil res. (Ω)	57	32
Wire length (m)	3	1.68

Samarium-Cobalt magnet; $\mu_0 M_0$=1.02 T
Coil: 280 turns of #47 wire; Current=0.05A

Fig. 6 Experimental setup and parameters

Table 2 Parameters of the equivalent SL models

	Parameters	Large	Small
PM (DMP) [6]	δ	0.3140	0.3122
(k=2; n=6)	m_j (μT/m^2)*	1.65, 0.02, 3.80	0.43, 0.02, 1.07
ESL model of	a_e (mm)	1.8168	1.456
the coil	$J_e d_w$ (A/m)	2.2750 e-5	3.8975 e-5

*m_j, j=1, 2, 3.

Table 3: Maximum difference from published experimental data

	Multilayer (%)	Single layer (%)
Tangential / Axial force	5.79 / 8.21	3.57 / 8.14

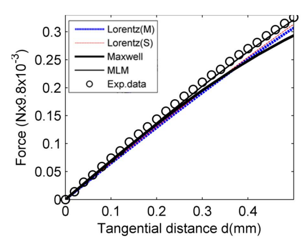

(a) Tangential forces (large)

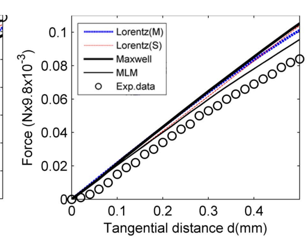

(b) Tangential forces (small)

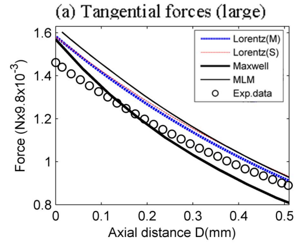

(c) Axial forces (large)

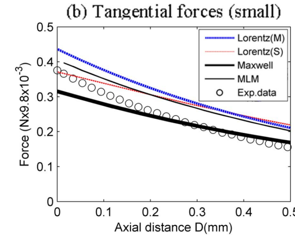

(d) Axial forces (small)

Fig. 7 Comparison between computed and experimental results

1-4244-1264-1/07/$25.00 ©2007 IEEE

IV. ILLUSTRATIVE APPLICATIONS

Two examples have been simulated. Example 1 investigates the effect of pole-shapes on the magnetic torque using DMP of the coils. Example 2 illustrates the **B**-fields to determine the orientation of a spherical motor.

Example 1: Effect of pole-shape and design configuration

Pole-shape designs have significant influences on the performance of an EM actuator. This example analyzes the effects of two pole-shapes on the torque of a spherical motor:

Design A [16] consists of 2 rows of 8 cylindrical PM's of γ =1.

Design B [17] uses 8 assemblies of 5 cylindrical PM's.

We focus on comparing net magnetic torques per unit magnet-volume for a given rotor radius and under the same influence of the stator coils in Fig 10. Detailed geometries of the PM pole-shapes are compared in Table 4 and Fig. 8.

Table 4 Parameters used in simulation

Common Parameters

Rotor radius, mm	Stator EM (θ_s=26°) OD×ID×L (mm)	# of turns	Current (Amp)	Air gap Mm
r_1=37.5	19.05×9.53×25.4	1050	±1	0.5

PM Pole Designs

Design	$\mu_0 M_0$ (T)	PM pole shape (mm)	Vol. (cm^3)
A	1.27	$2a = \ell = 12.7$, θ_r=20°	3.22
B	1.27	OD×L: 25×10, 20×5, 16×6, 12×3, 8×3	8.2

Simulated magnetic flux and potential lines are compared in Fig. 9; the potential and flux lines are orthogonal. Figure 9(a), or the left column, compares the magnetic fields of the PM only. Unlike *Design B* where only one (row of) PM is used, a significant portion of the flux lines in *Design A* forms a closed path between two PM's. Once the magnetic field of the PM's is found the force acting on the current-carrying loops can be calculated using the Lorentz force equation. Figure 10 compares the torque per unit volume of the two designs, which uses the magnetic field given in Fig. 9(a). In calculating the torques, ±1A current profiles in Fig. 10(a) are given to the coils such that a positive torque in +y-direction is generated.

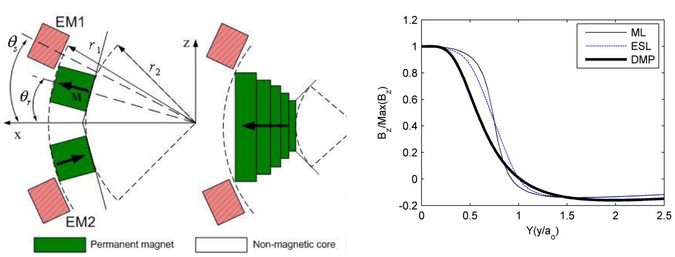

Design A Design B Normalized 2D B_z (PM: Design A)

Fig. 8 PM pole-shape designs

Figure 10(b) shows that *Design A* offers the larger magnetic to mechanical energy conversion than *Design B*. These observations can be explained by comparing the magnetic fields of the designs. As an illustration, snap-shots of the combined (PM and coil) field for the designs are compared in Fig. 9(b). In other words, the upper EM is repulsive while the lower EM is attractive. The comparison shows that *Design A* has significantly less leakage fluxes in the attractive PM or coil, and less attractive fluxes in the repulsive coil than *Design B*. The leakage fluxes in the attractive PM or coil are considered losses as they do not contributes to mechanical torques. Due to the large exposed surfaces in *Design B*, a relatively strong closed path is formed between the repulsive coil and the single PM, which produces an opposing torque, and thus reduces the net torque. As illustrated in Figure 9(b), the closed-form solution of the DMP models can offer an inexpensive means to visualize and analyze the effect of the EM fields on the leakage and unexpected flux paths that have significant influences on the magnetic torque.

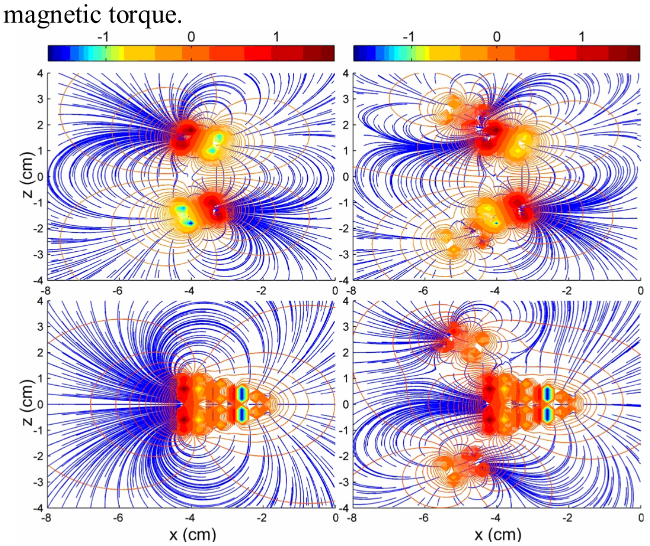

(a) PM only (b) Combined PM and EM (±1A)

Fig. 9 Magnetic fields (Orange line: potential; blue lines: magnetic flux) Top: Design A; bottom: Design B

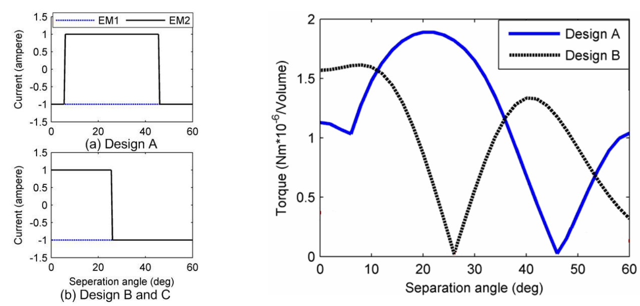

(a) current input (b) torque comparison

Fig. 10 Comparison of torque/volume

Example 2: Shaft Inclination Sensor

Figure 11 illustrates the use of DMP models [6] to determine the shaft inclination of a spherical motor by measuring the **B**-field of the cylindrical PM.

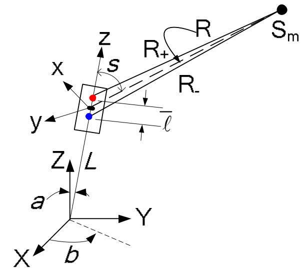

Sensor location:
S_1 = (a/2,0,b);
S_2= (-a/2,0,b);
S_3 = (0,a/2,b); and
S_4= (0,-a/2,b)
where a = 89mm (3.5in);
and b = 81mm (3.2in)

Fig. 11 Schematics Illustrating Inclination measurement

1-4244-1264-1/07/$25.00 ©2007 IEEE

The magnetic field of the PM at the m^{th} sensor located $\mathbf{S}_{\text{m}}$ can be calculated from (15):

$$\mathbf{B}=\frac{\mu_o}{4\pi}\sum_{j=0}^{k}m_j\sum_{i=1}^{n_k}\left(\frac{\mathbf{S_m}-(\mathbf{L}+\mathbf{p}_{ji+})}{\left|\mathbf{S_m}-(\mathbf{L}+\mathbf{p}_{ji+})\right|^3}-\frac{\mathbf{S_m}-(\mathbf{L}+\mathbf{p}_{ji-})}{\left|\mathbf{S_m}-(\mathbf{L}+\mathbf{p}_{ji-})\right|^3}\right) \quad (15)$$

where the distance vector $\mathbf{L}$ denotes the location of the PM in the reference XYZ frame

$$\mathbf{L}=L\left[\cos\alpha\cos\beta \quad \cos\alpha\sin\beta \quad \sin\beta\right]^{\mathrm{T}}; \quad (15a)$$

and the dipoles are known with respect to the coordinate frame *xyz* of the PM:

$$\mathbf{p}_{ji\pm}=\left[\bar{a}_j\cos i\theta \quad \bar{a}_j\sin i\theta \quad \pm\bar{\ell}/2\right]^{\mathrm{T}} \quad (15b)$$

Equation (15) provides a means to determine the unknown orientation $\mathbf{q}(\alpha, \beta)$ from the magnetic flux density $\mathbf{B}$ using Hall-effect sensors.

As an illustration, we consider a two-sensor-pairs array on the plane $Z_s=L$ such that the magnetic flux densities B_X and B_Y along the X and Y directions can be measured by the sensor pair $\mathbf{S}_1$ and $\mathbf{S}_2$ and the sensor pair $\mathbf{S}_3$ and $\mathbf{S}_4$ respectively. Figure 12(a) simulates the B fields measured by one of the sensors. Once the magnetic flux density $\mathbf{B}$ is known, the incremental change in orientation for real time ($\hat{\mathbf{q}}=\mathbf{q}_{k+1}-\mathbf{q}_k$, where the subscripts denote the time steps) can be computed from the linear equation (16):

$$\left[\mathbf{A}\right]\hat{\mathbf{q}}=\mathbf{b} \quad (16)$$

where $$\mathbf{b}=\left[\mathbf{B}(\mathbf{q}_{k+1})-\mathbf{B}(\mathbf{q}_k)\right]\in\mathbb{R}^{4\times1} \quad (16a)$$

and $$\left[\mathbf{A}\right]=\left[\left.\frac{\partial\mathbf{B}}{\partial\alpha}\right|_{\mathbf{q}=\mathbf{q}_k} \quad \left.\frac{\partial\mathbf{B}}{\partial\beta}\right|_{\mathbf{q}=\mathbf{q}_k}\right]\in\mathbb{R}^{4\times2} \quad (16b)$$

Figure 12(b) compares the estimated angles based on the incremental motion (16) against the exact solutions. In this simulation, the inclined shaft rotates about the Z-axis at 167 rpm and the sensor updates the measurements four times per revolution.

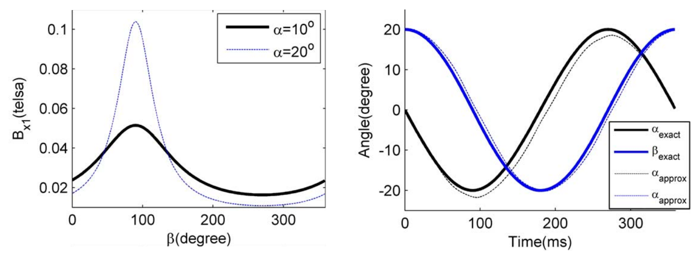

(a) Example simulated B-fields (b) Orientation comparison

Fig.12

V. CONCLUSIONS

Two different equivalent models for calculating the magnetic field and forces due to multilayer (ML) voice coils have been presented and validated; namely, an equivalent single layer (ESL) model, and an equivalent PM model. We have investigated the effects of coil geometry on the modeling errors, and also compared the Lorentz forces computed based on both the fields of the original ML coil and the ESL model. The comparisons are in excellent agreement; more importantly, computation with the ESL model requires only 5% of the computation time with the original ML coil in MATLAB. Through two illustrative applications, we demonstrate the use of the equivalent models for pole-shape design and field-based orientation sensing. Unlike numerical solutions such as FEM, the magnetic field solutions obtained using the equivalent PM model are in closed form and thus well suit for real-time computational applications.

REFERENCES

[1] Lee, K.-M. and C. Kwan, "Design concept development of a spherical stepper for robotic applications", *IEEE Trans. on Robotics and Automation*, 1991. p 75-181.

[2] Hollis, R. L., S. E. Salcudean, and A. P. Allan, "A six-degree-of-freedom magnetically levitated variable compliance fine-motion wrist: design, modeling, and control", *IEEE Trans. Robot. Automation*, 1991.p. 320-332.

[3] Wang, J., G. Jewell, and D. Howe, "Design and control of a novel spherical permanent magnet acutator with three degrees of freedom", *IEEE/ASME Trans. on Mechatronics*, 2003, p. 457.

[4] Liang, Y., I. M. Chen, G. Yang, L. Wei, and K.-M. Lee, "Analytical and experimental Investigation on the Magnetic Field and torque of a Permanent Magnet Spherical Actuator," *IEEE/ASME Trans. on Mechatronics*, 2006.

[5] Lee, K.-M. R. A. Sosseh and Z. Wei, "Effects of the Torque Model on the Control of a VR Spherical Motor," *IFAC Journal of Control Engineering Practice,* 2004. p 1437-1449.

[6] H. Son and K.-M. Lee "Distributed multi-pole model for motion simulation of PM-base spherical motor" submitted in AIM 2007.

[7] David K. Cheng "Field and wave electromagnetics" Addison Wesley 2nd edition p. 234-241.

[8] Craik, D. J., "Magnetostatics of axially symmetric structure", *J. of Physics*, 1974. p. 1566.

[9] Green, M. A., "Modeling the behavior of oriented permanent magnet material using current doublet theory", *IEEE Trans. on Magnetics*, 1988. p. 1528.

[10] Bennett, W. S., "Basic sources of electric and magnetic fields newly examined", *IEEE Antennas and Propagation Magazine*, 2001.p. 31-35.

[11] Nedelcu, S. and J. H. P. Watson, "Mangetic dipole model of a permanent magnet based device", *J. of Physics*, 2001. p. 2622-2628.

[12] Visschere, D. and R. Patrick, "An exact two-dimensional model for a periodic circular array of head-to-head permanent magnets", *J. of Physics D: Applied Physics*, 2005. p. 355-362.

[13] Jackson, J.D. "Classical electrodynamics " New York : Wiley, 1999

[14] Li, Qiang and K.-M. Lee, "An adaptive meshless computation method for design of electromechanical cctuators," *IEEE Trans. on Magnetics*, 2006, p. 1996-2002.

[15] Bastos, N. I. J. P. A. "Forces in permanent magnets team workshop problem 23," http://www.compumag.co.uk/team.html.

[16] Lee, K.-M. and H. Son. "Torque model for design and control of a spherical wheel motor", IEEE/ASME AIM2005 Proc. p. 335-340.

[17] Liang, Y., I-M. Chen, C. K. Lim, G. Yang, W. Lin, K-M. Lee, "Experimental Investigation on the Magnetic Field of a Permanent Magnet Spherical Actuator," IEEE/ASME AIM 2005. p. 347-352.

1-4244-1264-1/07/$25.00 ©2007 IEEE